(Received 28 August 2024, Accepted 22 October 2024, Scheduled 31 October 2024)

A Dual-Band High-Isolated MIMO Antenna Based on Compensation Network for 5G Coal Mine Applications

Yanhong Xu[1,*], Nanyue Li[1], Can Cui[2], Xuhui Fan[2], Jianqiang Hou[2], and Anyi Wang[1]

[1] *Xi'an Key Laboratory of Network Convergence Communication, College of Communication and Information Engineering Xi'an University of Science and Technology, Xi'an 710054, China*
[2] *National Key Laboratory of Science and Technology on Antenna and Microwave, Xidian University, Xi'an 710071, China*

ABSTRACT: A dual-band MIMO antenna with high isolation is designed in this paper for coal mine applications. Each of the two elements in the designed MIMO antenna is composed of a bident-shaped monopole structure which is designed to cover the 5G NR frequency region (2.51–2.67 GHz, 3.4–3.6 GHz) allocated for coal mine scenario. The two elements are symmetrically placed to achieve high isolation at lower frequency region with an element spacing of 0.09λ at the lowest operating frequency. To further reduce the mutual coupling between the two elements, the decoupling network technique is utilized. In particular, a neutralization line is loaded with an adjustable capacitor and two adjustable inductors on the ground. In this way, an isolation of higher than 20 dB is achieved over the two operating frequency bands for the MIMO antenna, i.e., the isolation is increased by more than 11 dB and 10 dB for the lower and higher bands, respectively. Besides, the good performance of the designed MIMO antenna in terms of correlation values and diversity gain makes it a suitable candidate for 5G MIMO applications under coal mine scenarios.

1. INTRODUCTION

With the development of intellectualization and digitalization, 5G technique with the advantages of high date rate, low latency, and large-scale device connectivity has been gradually applied in coal mine applications [1, 2]. Practically, the transmission of electromagnetic waves in underground environment usually faces severe multipath fading [3]. As one of the key techniques in 5G, Multiple-Input Multiple-Output (MIMO) technology has the ability to combat the negative effects of multipath fading and improve the reliability of wireless communication systems [4, 5]. Nevertheless, due to limited space reserved for antenna component, the mutual coupling is always strong between the elements in MIMO antenna, which would distort the performance of communication systems [6, 7].

Currently, various methods have been employed to achieve high isolation between MIMO antenna elements, such as adopting parasitic branch, defect ground structure (DGSs), neutralizing line, compensation network, and utilizing pattern diversity. Parasitic branch decoupling method utilizes the induced inverse current by the parasitic branch to cancel the coupling current between elements [8–11]. In particular, an 8-element dual-band MIMO antenna operating in the 5G New Radio band n77 (3300–4200 MHz) and 5 GHz band (4800–5000 MHz) in mobile handsets is presented in [8], where a T-shaped decoupling stub is utilized to achieve good mutual coupling reduction. In [10], a dual-band monopole antenna for 5G applications is presented, where a DGS and a T-shaped parasitic element are loaded to respectively reduce the mutual coupling of the lower (3.409–3.601 GHz) and higher (4.76–5.04 GHz) bands. For DGS decoupling method, different shapes are etched out of the ground to alter the surface current distribution on the ground to improve the isolation [12–17]. Specifically, a dual-band inverted-F MIMO antenna is designed for WLAN applications [12], where a high isolation over 15 dB is achieved by etching T-shaped slots out of the ground. In [13], a DGS consisting of a slant square loop structure with a T-shaped slit and a U-shaped slot is designed to realize high isolation of over 17.96 dB. However, this method usually not only affects the impedance matching of the antenna but also may damage the performance of antenna radiation pattern. Different from parasitic branch method, the neutralizing line method introduces a neutralizing line to connect the elements to achieve decoupling [18, 19]. In specific, a vertical T-shaped neutralization line is inserted between the antenna elements to obtain isolation greater than 16.5 dB [18]. In [19], an 8-element antenna array at 3.5 GHz for MIMO wireless application is designed, where the neutralization line and ground middle slot are used for decoupling the antenna elements in the array. Nevertheless, the design of the neutralizing line structure is complex. In the compensation network method, a new network with opposite characteristics to the original network is introduced to lower the mutual coupling between elements in MIMO antenna [20–22]. In particular, the proposed approach uses simple T-shaped networks where decoupling is realized, and the isolation is more than 15 dB [21]. This decoupling network method has the advantages of a simple design, high tunability, and excellent decoupling performance. In addition, pattern diversity is explored in [23] to design a dual-band (3.06–3.81 GHz and 3.33–3.67 GHz) high-isolated MIMO an-

* Corresponding author: Yanhong Xu (yanhongxuxidian@163.com).

tenna for 5G mobile terminals, and an isolation of higher than 14 dB is achieved in the overlapping bandwidth.

In this paper, we intend to design a dual-band high-isolated MIMO antenna for 5G NR coal mine applications by utilizing the compensation network. In particular, the dual bands of 2.4–2.67 GHz and 3.22–3.73 GHz assigned for 5G NR are realized with a bident-shaped monopole structure where an L-shaped branch of resonant frequency of 2.53 GHz and a monopole rectangular branch of 3.47 GHz are designed [24]. Note that the two elements in the MIMO antenna are symmetrically placed to enlarge the edge-to-edge space of the two L-shaped branches. To further increase the isolation between the two elements, a compensation network is designed, which is composed of an adjustable capacitor and two adjustable inductors located on a branch between the two elements. The proposed antenna exhibits excellent isolation of better than 20 dB in dual bands.

2. DECOUPLING PRINCIPLE

As depicted in Figure 1(a), the relationship between the two elements of a MIMO antenna is viewed as a network. After analyzing the characteristic of this network, a parallel compensating network with opposite characteristic is introduced as shown in Figure 1(b), and the resultant network is provided in Figure 1(c).

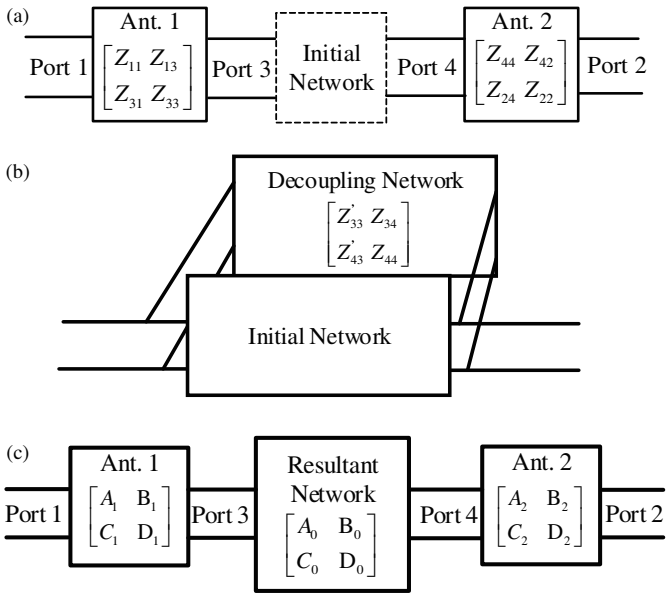

FIGURE 1. (a) Initial network of two elements, (b) illustration of parallel compensating network introduced to the initial network, and (c) resultant network.

The appropriate compensating network is chosen through the following theoretical analysis [25]. Eq. (1) can be used to depict the resultant network of Figure 1(c).

$$\begin{bmatrix} A_1 & B_1 \\ C_1 & D_1 \end{bmatrix} \cdot \begin{bmatrix} A_0 & B_0 \\ C_0 & D_0 \end{bmatrix} \cdot \begin{bmatrix} A_2 & B_2 \\ C_2 & D_2 \end{bmatrix} = \begin{bmatrix} A & B \\ C & D \end{bmatrix} \quad (1)$$

The relationship between the $ABCD$ matrix and Z parameters is as follows:

$$\begin{bmatrix} A_1 & B_1 \\ C_1 & D_1 \end{bmatrix} = \begin{bmatrix} \frac{Z_{11}}{Z_{31}} & \frac{Z_{11}Z_{33}-Z_{13}Z_{31}}{Z_{31}} \\ \frac{1}{Z_{31}} & \frac{Z_{33}}{Z_{31}} \end{bmatrix} \quad (2)$$

$$\begin{bmatrix} A_2 & B_2 \\ C_2 & D_2 \end{bmatrix} = \begin{bmatrix} \frac{Z_{44}}{Z_{24}} & \frac{Z_{44}Z_{22}-Z_{42}Z_{24}}{Z_{24}} \\ \frac{1}{Z_{24}} & \frac{Z_{22}}{Z_{24}} \end{bmatrix} \quad (3)$$

$$\begin{bmatrix} A_0 & B_0 \\ C_0 & D_0 \end{bmatrix} = \begin{bmatrix} \frac{Z_{33}}{Z_{43}} & \frac{Z_{33}Z_{44}-Z_{34}Z_{43}}{Z_{43}} \\ \frac{1}{Z_{43}} & \frac{Z_{44}}{Z_{43}} \end{bmatrix} \quad (4)$$

$$\begin{bmatrix} A & B \\ C & D \end{bmatrix} = \begin{bmatrix} \frac{Z_{11}}{Z_{21}} & \frac{Z_{11}Z_{22}-Z_{12}Z_{21}}{Z_{21}} \\ \frac{1}{Z_{21}} & \frac{Z_{22}}{Z_{21}} \end{bmatrix} \quad (5)$$

Note that the ABCD matrices of Ant. 1 and Ant. 4 are known. Our goal is to achieve the decoupling between these two elements while maintaining impedance matching, i.e., the Z-parameter matrix of the resultant network needs to satisfy the following objective:

$$\begin{bmatrix} Z'_{11} & Z'_{12} \\ Z'_{21} & Z'_{22} \end{bmatrix} = \begin{bmatrix} 50 & 0 \\ 0 & 50 \end{bmatrix} \quad (6)$$

According to Eq. (6), the $ABCD$ matrix of the MIMO antenna can be easily obtained. In the sequel, the desired $ABCD$ matrix of resultant network is calculated according to Eq. (1). The impedance characteristic of the desired compensating network can be obtained based on the relation shape of $ABCD$ matrix and Z matrix.

3. ANTENNA DESIGN

3.1. Structure of the Dual-Band MIMO Antenna

Figure 2 provides the top perspective of the dual-band MIMO antenna, termed as Ant. 1. From this figure, it can be seen that the antenna consists of two symmetrical radiating elements and a partial ground plane separately placed on the upper and lower sides of a 1.6mm-thick FR4 substrate with $\varepsilon_r = 4.4$ and

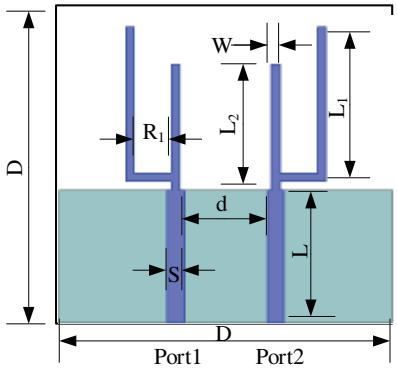

FIGURE 2. Top view of dual-band MIMO antenna (Ant.1), where $D = 40$, $S = 16$, $L = 16$, $L_1 = 18.5$, $L_2 = 15$, $W = 1$, $R_1 = 4.5$, and $d = 12$ in mm.

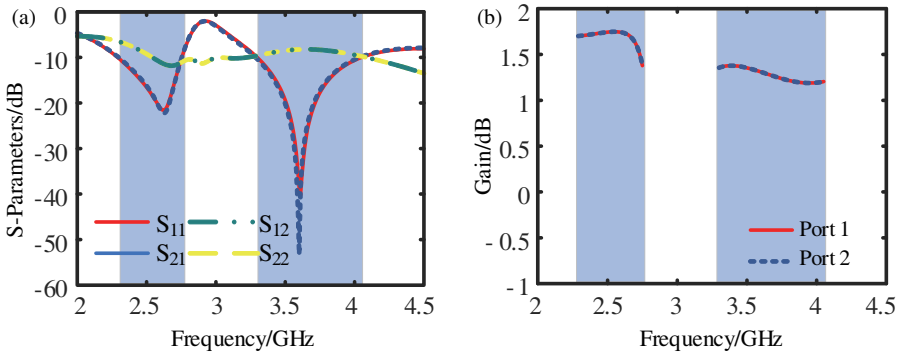

FIGURE 3. Simulated (a) S parameters and (b) gain of the MIMO antenna in Figure 2.

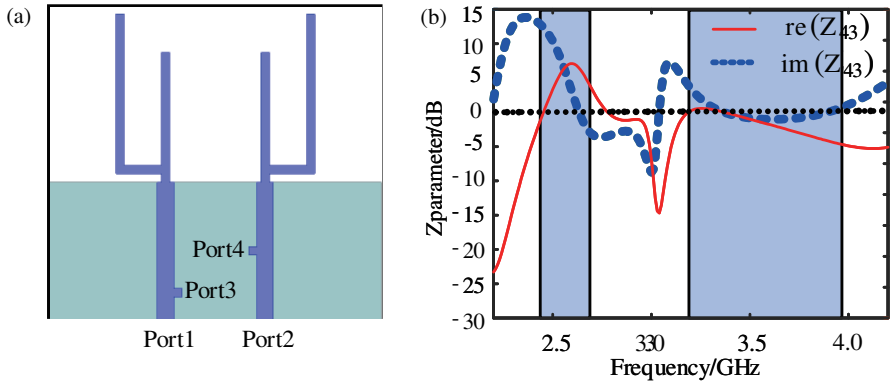

FIGURE 4. (a) Dual-band MIMO antenna with two auxiliary ports. (b) Real and imaginary parts of Z_{43}.

$\tan\delta = 0.02$, on the lower side of the substrate, and a dielectric substrate. The two ports are 12 mm apart. The optimized parameters of the antenna are also provided in the caption of Figure 2.

Figure 3 presents the simulated S parameters, and gain of the MIMO antenna in Figure 2. From Figure 3(a), it can be observed that the antenna operates in two frequency bands, i.e., 2.29–2.75 and 3.3–4.05 GHz. Meanwhile, we can see that the mutual coupling is strong, and the isolation of the entire frequency regions is higher than -11 dB. From Figure 3(b), it is seen that the antenna exhibits a gain greater than 1.2 dBi at the two operating frequency regions.

To reduce the mutual coupling effects between the two elements, two auxiliary ports 3 and 4 are introduced to analyze the characteristics of the initial network according to Eq. (1). Figure 4 provides the dual-band MIMO antenna with two auxiliary ports and the real and imaginary parts of the impedance between these two ports. Figure 4(b) depicts the impedance diagram of the antenna, where the original network exhibits capacitive characteristics when $Z < 0$ and inductive characteristics when $Z > 0$. As depicted in this figure, it is observed that the initial network exhibits a capacitive behavior within the frequency range from 3.22 to 3.73 GHz, while exhibits an inductive behavior within the frequency range of 2.4 to 2.67 GHz.

3.2. Design of Dual-Band MIMO Antenna with High Isolation

On the basis of the analysis of Subsection 3.1, the compensation network is designed to improve the isolation level between the two elements. The compensation network consists of a neutralizing line, a capacitor to compensate the inductive characteristic at the lower frequency band, and two inductors to compensate capacitive characteristic at the upper frequency band. By adjusting the values of the capacitor and inductors, the decoupling effect can be optimized. Figure 5 provides the top view of the proposed dual-band high-isolated MIMO antenna and evolution procedures of the decoupling network, and the proposed antenna is termed as Ant. 4, along with the optimized parameters listed in its caption.

As aforementioned, the spacing between the two elements is 12 mm (0.09λ at 2.4 GHz). The performance of Ant. 1 is significantly deteriorated due to the strong mutual coupling. Figure 6 provides the S_{21} parameters of Ant. 1 and Ant. 2. From this figure, it can be seen that the mutual coupling in the two bands is greatly reduced after adopting the optimized compensation network. In specific, the amplitude of S_{21} can be as high as -10 dB before mutual coupling compensation. After adopting the optimized compensation network, the S_{21} is lowered to -21 dB and -23 dB at the lower and upper bands, respectively.

In the following, the influence of inductor of T_1 and capacitor of C_1 on antenna performance is investigated. Figure 7 provides the S_{21} curves verses the values of T_1 and C_1, from which it can be seen that the S_{21} value at lower frequency band is primarily influenced by the inductor, while the S_{21} value at upper frequency band is primarily influenced by the capacitor. To achieve a higher isolation at both bands, T_1 is set to 33 nH, and C_1 is set to 0.25 pF.

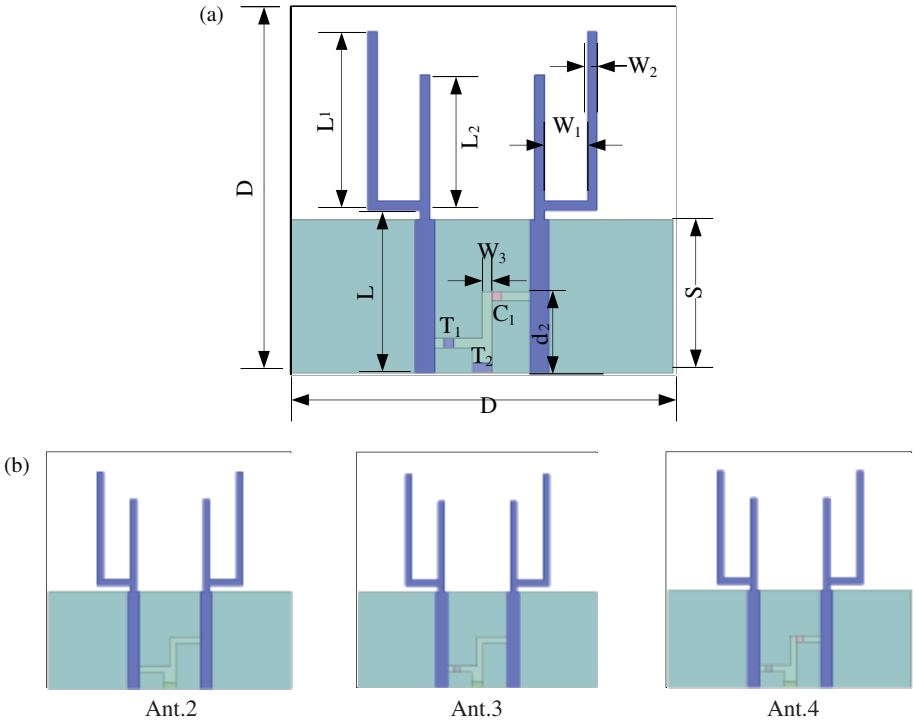

FIGURE 5. Top view of proposed dual-band high-isolated MIMO antenna (Ant. 4) with $D = 40$, $S = 16$, $L = 16$, $L_1 = 18.5$, $L_2 = 15$, $W_1 = 4.5$, $W_2 = 1$, $W_3 = 1$, and $d_2 = 7.5$ in mm, and $C_1 = 0.25$ pF, $T_1 = 2.2$ nH, $T_2 = 33$ nH, (b) Evolution procedures of the dual-band MIMO antenna decoupling.

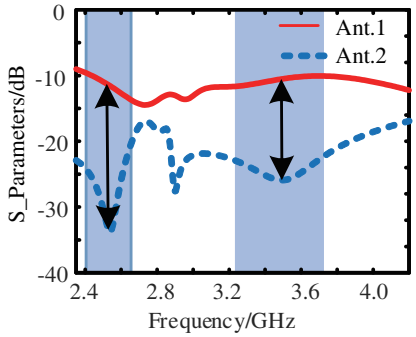

FIGURE 6. S_{21}-parameter curves of Ant. 1 and Ant. 2.

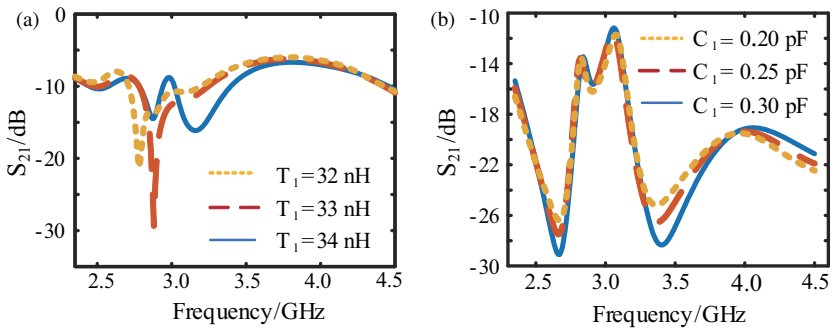

FIGURE 7. S_{21} with respect to (a) T_1, (b) C_1.

To further show the decoupling effects after adopting the compensation network, the simulated current distributions at the center frequency of these two bands, i.e., 2.53 and 3.47 GHz, are provided in Figure 8. Port 2 is excited, while a matched load is connected to port 1. From Figure 8, it is seen that a strong coupled current is observed on Ant. 1 at both frequencies, while the coupled current is greatly reduced after adopting the designed network on Ant. 4.

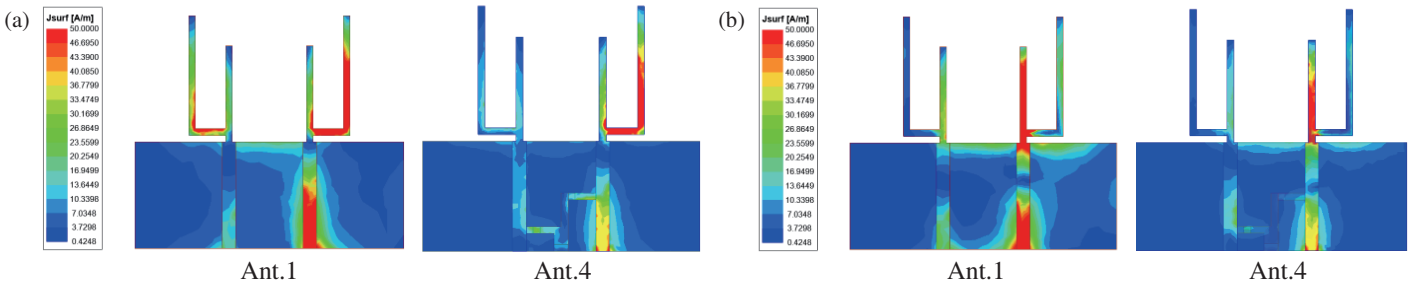

FIGURE 8. Simulated current distributions of Ant. 1 and Ant. 4 at (a) 2.53, and (b) 3.47 GHz.

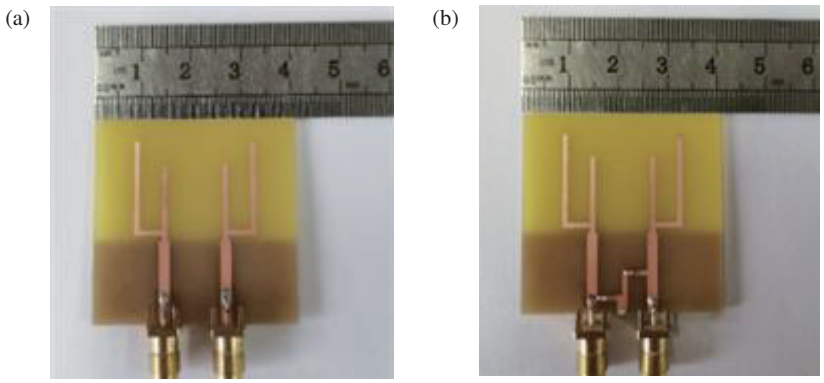

FIGURE 9. Prototypes of (a) Ant. 1 and (b) Ant. 4.

4. SIMULATED AND MEASURED RESULTS

To demonstrate the performance of the designed antenna, prototypes of Ant. 1 and Ant. 4 are both fabricated as depicted in Figure 9. The prototypes are measured with an Agilent N5244A network analyzer.

In the measurement, only S_{11} and S_{21} are measured since Port 1 and Port 2 are reciprocal. The measured and simulated S-parameters are provided in Figure 10(a). Good agreement is observed between the measured and simulated results. The isolation between the antenna elements exceeds 20 dB, which is more than a 10 dB improvement compared to the pre-decoupling antenna isolation. In a MIMO antenna system, the envelope correlation coefficient (ECC) is typically adopted to quantify the correlation between the envelopes of multiple antenna-received signals. In practical scenarios, it is desirable for the ECC level to remain below 0.5. The ECC value of the designed antenna is calculated using Eq. (7), where q_{sml} is the complex coefficient of the spherical harmonic; the order m ($-l \leq m \leq l$) describes the azimuthal variation of the field; the variation in elevation depends on the degree l and the order m; the index $s \in \{1, 2\}$ is connected with the components of transversal electric and transversal magnetic waves; $(\cdot)^*$ stands for the complex conjugate [26] and is provided in Figure 10(b), from which it can be seen that the ECC is less than 0.04 dB across the two frequency bands.

$$\mathrm{ECC} = \frac{\sum_{l=1}^{\infty}\sum_{m=-1}^{l}\sum_{s=1}^{2} q_{sml}^{1}(q_{sml}^{2})^{*}}{\sqrt{\left(\sum_{l=1}^{\infty}\sum_{m=-1}^{l}\sum_{s=1}^{2} q_{sml}^{1}(q_{sml}^{1})^{*}\right)\left(\sum_{l=1}^{\infty}\sum_{m=-1}^{l}\sum_{s=1}^{2} q_{sml}^{2}(q_{sml}^{2})^{*}\right)}} \tag{7}$$

Diversity gain (DG) is another performance metric for the mutual isolation or correlation degree of the communication channels, which should be as close to 10 dB as possible. The calculation formula for DG is provided in Eq. (8), and the DG of the designed antenna is approximately 9.98 dB as can be seen from Figure 10(c). Meanwhile, it can be observed that the consistency between the simulated and measured data is quite good, indicating good diversity performance.

$$\mathrm{DG} = 10 \times \sqrt{1 - \rho_e^2} \tag{8}$$

Figure 10(d) displays the simulated and measured radiation patterns of the designed antenna. It can be observed from the figure that the proposed antenna exhibits approximately 8-shaped and omnidirectional radiation patterns respectively in E- and H-planes at either of the two operating frequencies. Moreover, the measured radiation patterns of the antenna exhibit good consistency with the simulated ones.

Mean Effective Gain (MEG) is employed to further quantify the relationship between the average received power and average incident power of measured antennas, which can be calcu-

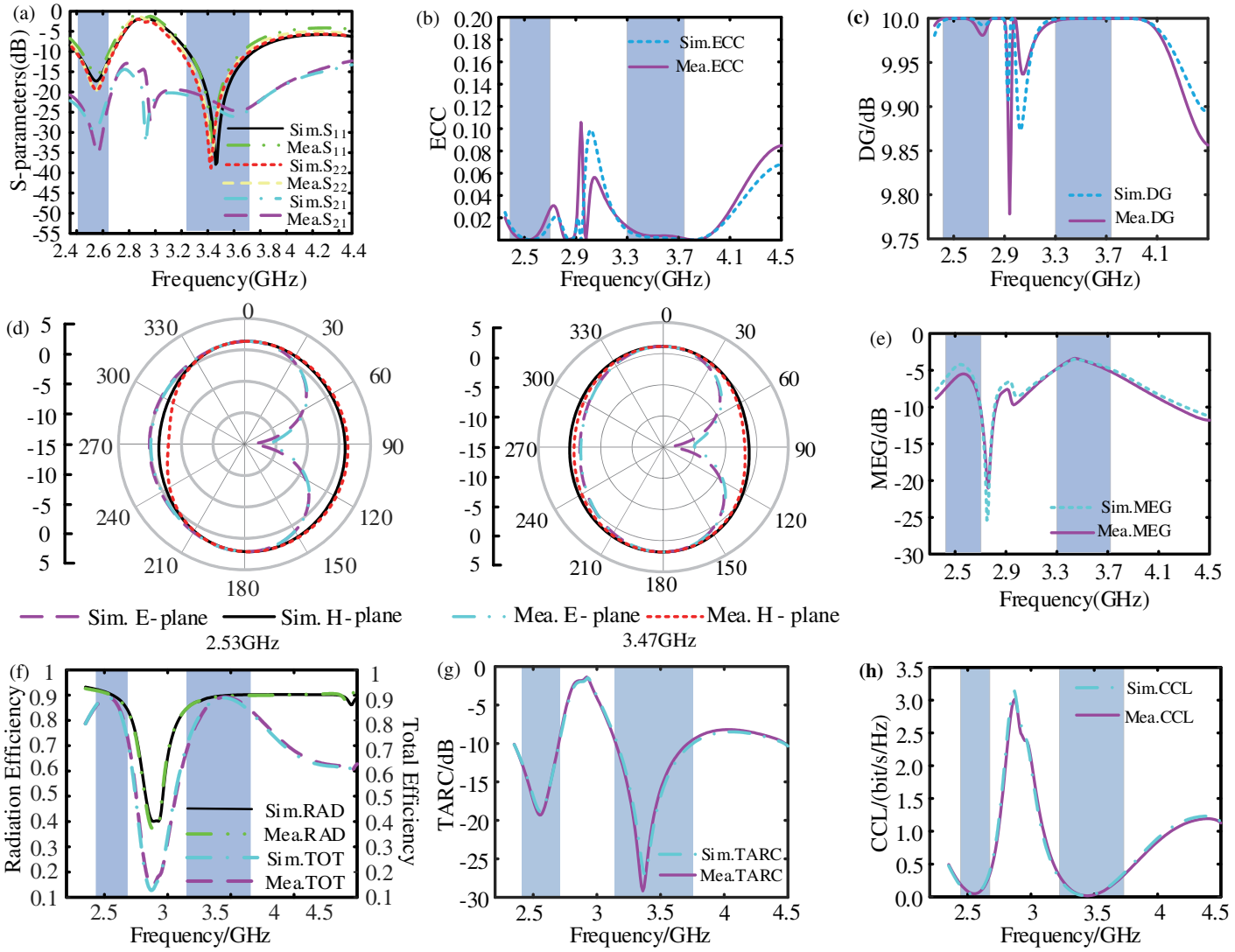

FIGURE 10. Simulated and measured (a) S-parameters, (b) ECCs, (c) DGs, (d) radiation patterns, (e) MEGs, (f) Efficiencies, (g) TARCs, and (h) CCLs.

lated by Eq. (9), and the result of the MEG should be within a range between -3 and -12 dB. The simulated and measured data of MEG are depicted in Figure 10(e), where the MEG ranges between -4 dB and -10 dB.

$$\text{MEG} = 0.5 \times \left(1 - \sum_{i=1}^{N} |S_{ij}|\right) \tag{9}$$

where N represents the number of elements in MIMO antenna.

The simulated and measured radiation efficiencies and total efficiencies are given in Figure 10(f). As shown in Figure 10(f), it is seen that the simulated and measured antenna radiation efficiencies are both better than 85%, and total efficiencies are all better than 75%.

Total Active Reflection Coefficient (TARC) is to be evaluated, which relates the total incident power and reflected power in the multi-antenna environment. For a two-port network, based on S-parameter, TARC is given by Eq. (10) [27, 28], and the TARC is less than -10 dB in the operating frequency range as can be seen from Figure 10(g). Meanwhile, it can be observed that the consistency between the simulated and measured data is quite good, and hence this antenna system is claimed to be efficient in MIMO environment.

$$TARC = -\sqrt{\frac{(S_{11} + S_{12})^2 + (S_{22} + S_{21})^2}{2}} \tag{10}$$

Channel Capacity Loss (CCL) signifies the capacity or capability of the channel to accommodate the bandwidth, for the two-port MIMO structure, the CCL in terms of S-parameters is given in Eqs. (11)–(13) [29, 31]. CCL is to be $\backslash 0.4$ bits/s/Hz for better performance, and from Figure 10(h), for the proposed antenna it is $\backslash 0.3$ bits/s/Hz in the operating frequency range of the antenna.

$$\text{CCL} = -\log_2 \det\left(\partial^M\right) \tag{11}$$

$$\partial^M = \begin{bmatrix} \partial_{11} & \partial_{12} \\ \partial_{21} & \partial_{22} \end{bmatrix} \tag{12}$$

TABLE 1. Performance comparisons of reported MIMO antennas.

Reference	Decoupling Method	Bandwidth (GHz)	Space (λ)	Isolation (dB)	Efficiency (%)
[8]	Strip and DGS	3.30–5.95	0.30	> 15.0	> 47
[14]	Polarization orthogonal	3.4–3.6, 4.8–4.9	0.17	> 16.8 > 11.8	> 45.7 > 42.6
[15]	Spiro-Meander line EBG	5.5–6.1	0.14	> 19.0	> 40
[17]	Neutralization line and ground middle slot	3.40–3.60	0.17	> 16.0	> 40
[22]	Differential feed	3.06–3.81, 3.33–3.67	0.28	> 14.0	> 52
[23]	Two sets of three modes with different weightings	3.25–3.92	0.11	> 14.3	> 73
Prop.	Compensation network	2.4–2.67, 3.22–3.73	0.09	> 22.0	> 85

$$\begin{cases} \partial_{11} = 1 - \left(|S_{11}|^2\right) + \left(|S_{12}|^2\right) \\ \partial_{22} = 1 - \left(|S_{22}|^2\right) + \left(|S_{21}|^2\right) \\ \partial_{12} = -\left(S_{11}^* S_{12} + S_{12}^* S_{22}\right) \\ \partial_{21} = -\left(S_{22}^* S_{21} + S_{21}^* S_{11}\right) \end{cases} \tag{13}$$

Performance comparison of our work with several recently reported MIMO antennas are provides in Table 1. From Table 1, it can be seen that our work achieves a high isolation level of over 20 dB with the smallest element spacing and a higher efficiency of over 85%.

5. CONCLUSION

This paper presents a dual-band MIMO antenna with high isolation for coal mine applications. The proposed antenna can operate at two frequency bands of 2.4–2.67 GHz and 3.22–3.73 GHz, which can effectively cover the assigned 5G NR bands for coal mine. On the basis of the characteristic analysis of initial network at the above dual bands, an adjustable compensation network consisting of a capacitor and two inductors on a branch is designed and optimized. An isolation level of more than 20 dB is achieved at both of the operating frequency bands. The results show that the antenna has a low envelope correlation coefficient, a high diversity gain, and an appropriate mean effective gain, which make it a good candidate for coal mine applications.

ACKNOWLEDGEMENT

The authors would like to thank the editors and anonymous reviewers for their efforts in evaluating our manuscript.

This work was supported in part by the National Natural Science Foundation of China, Grants 62271386, 62301415, and 62301414, and in part by the Shanxi Science and Technology Association Youth Talent Lifting Program, Grant 20230149.

REFERENCES

[1] Li, T. and C. Zhuo, "Application and research of 5G communication technology in intelligent coal mine," *Journal of Electronic Research and Application*, Vol. 7, No. 4, 31–36, 2023.

[2] Wang, G., G. Zhao, and Y. Hu, "Application prospect of 5G technology in coal mine intelligence," *Journal of China Coal Society*, Vol. 45, No. 1, 16–23, 2020.

[3] Zhang, X. and C. D. Sarris, "Statistical modeling of electromagnetic wave propagation in tunnels with rough walls using the vector parabolic equation method," *IEEE Transactions on Antennas and Propagation*, Vol. 67, No. 4, 2645–2654, 2019.

[4] Kumar, A. and A. Chaudhary, "Channel capacity enhancement of wireless communication using MIMO technology," *International Journal of Scientific & Technology Research*, Vol. 1, No. 2, 10–15, 2012.

[5] Malviya, L., R. K. Panigrahi, and M. V. Kartikeyan, *MIMO Antennas for Wireless Communication: Theory and Design*, CRC Press, 2020.

[6] Chen, K.-H. and J.-F. Kiang, "Effect of mutual coupling on the channel capacity of MIMO systems," *IEEE Transactions on Vehicular Technology*, Vol. 65, No. 1, 398–403, 2016.

[7] Chen, X., S. Zhang, and Q. Li, "A review of mutual coupling in MIMO systems," *IEEE Access*, Vol. 6, 24 706–24 719, 2018.

[8] Cui, L., J. Guo, Y. Liu, and C.-Y.-D. Sim, "An 8-element dual-band MIMO antenna with decoupling stub for 5G smartphone applications," *IEEE Antennas and Wireless Propagation Letters*, Vol. 18, No. 10, 2095–2099, 2019.

[9] Gopal, K. V. and Y. S. Rao, "Mutual coupling reduction in UWB MIMO antenna using T-shaped stub," *Progress In Electromagnetics Research Letters*, Vol. 112, 77–85, 2023.

[10] Wang, W., Y. Wu, W. Wang, and Y. Yang, "Isolation enhancement in dual-band monopole antenna for 5G applications," *IEEE Transactions on Circuits and Systems II: Express Briefs*, Vol. 68, No. 6, 1867–1871, 2021.

[11] Xu, Y., P. Dong, and A. Wang, "Design of a high isolation tri-band MIMO antenna for coal mine applications," *Journal of Electromagnetic Waves and Applications*, Vol. 37, No. 13, 1106–1121, 2023.

[12] Deng, J., J. Li, L. Zhao, and L. Guo, "A dual-band inverted-F MIMO antenna with enhanced isolation for WLAN applications," *IEEE Antennas and Wireless Propagation Letters*, Vol. 16, 2270–2273, 2017.

[13] Dong, G., J. Huang, Z. Chen, and G. Liu, "A compact planar dual band two-port MIMO antenna with high isolation and efficiency," *International Journal of RF and Microwave Computer-Aided Engineering*, Vol. 32, No. 8, e23245, 2022.

[14] Chang, L., G. Zhang, and H. Wang, "Dual-band antenna pair with lumped filters for 5G MIMO terminals," *IEEE Transactions on Antennas and Propagation*, Vol. 69, No. 9, 5413–5423, 2021.

[15] Kumar, N. and U. K. Kommuri, "MIMO antenna mutual coupling reduction for WLAN using spiro meander line UC-EBG," *Progress In Electromagnetics Research C*, Vol. 80, 65–77, 2018.

[16] Zhang, W., Y. Li, K. Wei, and Z. Zhang, "Dual-band decoupling for two back-to-back PIFAs," *IEEE Transactions on Antennas and Propagation*, Vol. 71, No. 3, 2802–2807, 2023.

[17] Cai, J., J. Huang, B. Chen, L. Shen, T. H. Loh, and G. Liu, "A defected circular ring dual-band MIMO antenna with high isolation for 5G and IEEE 802.11 a/ac/ax," *Progress In Electromagnetic Research M*, Vol. 113, 237–247, 2022.

[18] Dkiouak, A., M. E. Ouahabi, S. Chakkor, M. Baghouri, A. Zakriti, and Y. Lagmich, "High performance UWB MIMO antenna by using neutralization line technique," *Progress In Electromagnetics Research C*, Vol. 131, 185–195, 2023.

[19] Abdullah, M., Y.-L. Ban, K. Kang, M.-Y. Li, and M. Amin, "Eight-element antenna array at 3.5 GHz for MIMO wireless application," *Progress In Electromagnetics Research C*, Vol. 78, 209–216, 2017.

[20] Zhang, Y.-M., Q.-C. Ye, G. F. Pedersen, and S. Zhang, "A simple decoupling network with filtering response for patch antenna arrays," *IEEE Transactions on Antennas and Propagation*, Vol. 69, No. 11, 7427–7439, 2021.

[21] Hei, Y. Q., J. G. He, and W. T. Li, "Wideband decoupled 8-element MIMO antenna for 5G mobile terminal applications," *IEEE Antennas and Wireless Propagation Letters*, Vol. 20, No. 8, 1448–1452, 2021.

[22] Chiu, C.-Y., B. K. Lau, and R. Murch, "Bandwidth enhancement technique for broadside tri-modal patch antenna," *IEEE Open Journal of Antennas and Propagation*, Vol. 1, 524–533, 2020.

[23] Xu, Z. and C. Deng, "High-isolated MIMO antenna design based on pattern diversity for 5G mobile terminals," *IEEE Antennas and Wireless Propagation Letters*, Vol. 19, No. 3, 467–471, 2020.

[24] Emontsbotz, J. J., H. J. Lee, S. Schmitt, M. Brochhaus, A. Krishnan, J. L. Sieger, V. Jung, S. Brell-Cokcan, N. König, and R. H. Schmitt, "The application of 5G networks on construction sites and in underground mines: successful outcomes from field trials," in *2024 19th Wireless On-Demand Network Systems and Services Conference (WONS)*, 105–112, Chamonix, France, Jan. 2024.

[25] Sasamori, T. and T. Fukasawa, "S-parameter method and its application for antenna measurements," *IEICE Transactions on Communications*, Vol. 97, No. 10, 2011–2021, 2014.

[26] Alieldin, A., Y. Huang, M. Stanley, S. D. Joseph, and D. Lei, "A 5G MIMO antenna for broadcast and traffic communication topologies based on pseudo inverse synthesis," *IEEE Access*, Vol. 6, 65 935–65 944, 2018.

[27] Fritz-Andrade, E., H. Jardon-Aguilar, and J. A. Tirado-Mendez, "The correct application of total active reflection coefficient to evaluate MIMO antenna systems and its generalization to N ports," *International Journal of RF and Microwave Computer-Aided Engineering*, Vol. 30, No. 4, e22113, 2020.

[28] Addepalli, T., J. B. Kamili, S. Boddu, R. Manda, A. Nella, and B. K. Kumar, "A 4-element crescent shaped two-sided MIMO antenna for UWB, X and Ku band wireless applications," *Wireless Networks*, Vol. 29, No. 8, 3333–3348, 2023.

[29] Addepalli, T., M. Sharma, M. S. Kumar, N. K. Gollamudi, P. R. Kapula, and C. M. Kumar, "Self-isolated miniaturized four-port multiband 5G sub 6 GHz MIMO antenna exclusively for n77/n78 & n79 wireless band applications," *Wireless Networks*, Vol. 30, No. 2, 1037–1053, 2024.

[30] Addepalli, T., M. Sharma, A. Nella, A. P. Ambalgi, and P. R. Kapula, "Experimental investigation of super-wideband 8-port Multiple-Input-Multiple-Output antenna with high isolation for future wireless applications including Internet of Things," *International Journal of Communication Systems*, e5199, 2022.

[31] Sharma, M., T. Addepalli, R. Manda, T. Vidyavathi, and P. R. Kapula, "A detailed insight of 2×2 high isolation wideband dual notched band MIMO antenna with evolution initiated by theory of characteristics mode," *International Journal of Microwave and Wireless Technologies*, Vol. 15, No. 8, 1392–1411, 2023.